Numerical Investigation and Analysis of the Unsteady Supercavity Flows with a Strong Gas Jet

X. Y Zhao, M. Xiang, H. C. Zhou and W. H. Zhang[†]

College of Aerospace Science and Engineering, National University of Defense Technology, Changsha 410073, P.R. China

†*Corresponding Author Email: xiangmin333@hotmail.com*

ABSTRACT

Artificial supercavitation is one of the most prospective technique for underwater drag reduction, but it still faces some unsolved roadblocks, like cavity stability, noise, power etc. This article aims at investigating the instability of cavity with the strong jet impingement, and analyzing jet behavior in restricted space. A multiphase model using coupled VOF and level set method is adopted to capture the gas-liquid interface. By changing the position of jet nozzle exit and the jet intensity, a series of numerical simulation is performed. Firstly the transient evolution of the cavity interface under the effect of the high-speed jet is obtained. Numerical model is validated by comparing with the experimental data. Then the criterion to determine the transition between different jet/cavity interaction mechanisms is established based on a non-dimensional distance parameter. Furthermore, the entrainment mechanism inside the cavity is analyzed and provides useful insights on enhancing the cavity stability with strong jets.

Keywords: Jet, Supercavity; Instability; CLSVOF; Numerical research.

NOMENCLATURE

A	cross sectional area	Q_D	mass flow rate of the gas ventilation
a	turbulence coefficient	Q_R	reflux mass flow rate
Cx	drag coefficient of the cavitator	$\overline{S}_0$	non-dimensional distance parameter
Cq	gas ventilation coefficient	S_D	cone cavitator bottom area
Dc	maximum diameter of the supercavity	S_{jet}	nozzle exit area
Dn	cavitator diameter	U_∞	liquid flow velocity
Fr	Froude number	U_C	centerline axial mean velocity
g	gravity	U_{jet}	mean jet velocity at the nozzle exit
$\overline{J}$	non-dimensional number of the jet momentum flux	W_c	cavitator drag
Lc	length of the supercavity		
L_1	potential core length of the jet	$\pi\alpha$	half top angle of a cone
L_2	recirculation region length of the jet	α_g	volume fraction of the gas phase
$\dot{m}_{jet}$	mass flow rate of the jet	$\varphi(x,t)$	level-set function
$\overline{P}$	non-dimensional number of the ratio of the free-stream total pressure to that of the jet	ρ	density
p_∞	free liquid flow pressure	σ_c	cavitation number
p_C	pressure inside the supercavity		

1. INTRODUCTION

Cavitation is a dynamic phenomenon that occurs when underwater vehicles travel with such a high speed that the pressure around the vehicle surface decrease to the vapor saturation pressure of the liquid. High drag reduction could be achieved when the vehicle is entirely covered by the cavity which is defined as supercavitation. However,5 it is difficult to achieve supercavitation under natural conditions.

Reichardt (1946) firstly used the method of artificial air injection to form a steady cavity that covered the entire surface of an object. That pioneering work provided the possibility for engineering application of drag reduction by cavitation. Afterwards an amount of works that contain theoretical and experimental work on ventilated cavitation were performed. The empirical formulas of the stable cavity shape and the ventilation rate demand for supercavity formation without external perturbations have been built. In one word, ventilated cavity flows without jet mainly depends on several non-dimensional fundamental parameters: such as cavitation number, σ_c, Froude number, Fr, and the gas ventilation coefficient, Cq.

$$\sigma_c = \frac{2(p_\infty - p_c)}{\rho_\infty U_\infty^2} \tag{1}$$

$$Fr = \frac{U_\infty}{\sqrt{gD_n}} \tag{2}$$

$$C_q = \frac{Q_D}{\rho_\infty U_\infty D_n^2} \tag{3}$$

In those relation, p_∞, ρ_∞ and U_∞ denote the free liquid flow pressure, the liquid density and velocity respectively; p_c is the pressure inside the supercavity; Dn is the cavitator diameter; and Q_D refers to the gas ventilation mass flow rate.

In order to achieve high drag reduction efficiency, it is always required a stable cavity shape. However the cavitation stability could be disturbed by many factors. As the jet engine is considered as the most prospect propulsion system for the supercavitating vehicle, recently, the effects of the gas jet from exhaust nozzle on an established cavity has got more and more attention. Paryshev (2006) gave an approximate mathematical models of cavity when it closes on a central liquid or incompressible gas jet. According to his theory, the effect of jet on the cavity was governed by two non-dimensional numbers: $\bar{P}$, the ratio of the stagnation pressure of the surrounding flow to that of the jet, and $\bar{J}$, the ratio of the jet momentum flux to the cavitator drag, which are defined as follows:

$$\bar{P} = \frac{\rho_\infty U_\infty^2}{\rho_{jet} U_{jet}^2} \tag{4}$$

$$\bar{J} = \frac{\dot{m}_{jet} U_{jet}}{W_c} \tag{5}$$

Where U_{jet} denotes the mean jet velocity at the nozzle exit; $\dot{m}_{jet}$ denotes the mass flow rate of the jet; W_c is the cavitator drag. Jet/supercavity interaction is divided into three categories：① when $\bar{P} > 1$ and $\bar{J} < 1/2$, the jet is totally obstructed by the cavity, and returns into it. ② when $\bar{P} > 1$ and $\bar{J} > 1/2$, the jet is divided into two parts, a portion goes out of the cavity while the other portion returns and inflates the cavity. ③when $\bar{P} < 1$, the jet isn't completely obstructed and leaves the cavity. Money (2015) conducted a series of experiments on jet-supercavity interaction in the 1.22m dia. Garfield Thomas Water Tunnel. By changing the jet mass flow rates from 0 to 0.11kg/s, experiments were performed at two tunnel speeds and for two nozzle diameters. Collected data well supported Paryshev's theory models. Kinzel *et al.* (2017) used a high-fidelity CFD method to evaluate the modeling developed by Paryshev. CFD results were in consistent with the experimental data and showed that Paryshev's Model should be generalized to account for stagnation pressure losses of the jet. Xu Hao *et al.* (2018) carried out an experimental study on the supersonic gaseous jet induced tail cavity at the wake of a revolution body, and investigated the transient evolution characteristics and forming mechanism. According to the observation, the induced cavities had four forms: foamy, intact, partially break, and pulsating foamy closure type. About the recent research progress on the unsteady supercavity, Zou *et al.* (2010) gave a gas-leakage rate formula for the unsteady ventilated supercavity and verified its validity. Based on Logvinovich model, Zou *et al.* (2013) studied the relationship between the shedding frequency and the velocity disturbance for the unsteady supercavity flows. Karn *et al.* (2016) conducted an important study on closure mechanisms for the unsteady ventilated supercavity. These unstable closure modes were either observed at the transition of two stable closure modes or at superfluous ventilation rates. Sun *et al.* (2019) carried out a numerical investigation on the shedding mechanism for the ventilated partial cavitating flows, and analyzed how the vortex structures were created and developed in the cavity shedding process.

Considering that enough propulsion is always required to insure that underwater vehicles could run steadily in a high speed, we prefer to concern the supercavtiy flows with a strong gas jet that could provide thrust no less than the cavitator drag($\bar{J} > 1$, or $\bar{J} \approx 1$). With sufficient momentum, such cavities could experience instability, pulsation and collapse under certain circumstances. This article aims at investigating the instability of cavity with the strong jet impingement, and analyzing jet behavior in restricted space based on theoretical and numerical methods. Besides jet strength, the distance between the nozzle exit and cavity closure is considered as a very important parameter in jet/supercavity interaction. As the relative position varies, it may lead to diverse cavity surface evolution and different jet entrainment effect in cavity. In this paper, simulation for a supercavity case without jet will be firstly carried out under different ventilation flow rate and comparison with the experimental data will be carried out to validate the numerical model. Then, by changing jet nozzle exit, a series of numerical simulation will be performed. The effect of the relative position on the jet/cavity interaction will be analysed to provide useful methods in enhancing the stability of the ventilated cavity.

2. THEORETICAL ANALYSIS OF THE JET/CAVITY INTERACTION

2.1 Analysis of the Key Parameters

Parametric analysis is a necessary task before numerical simulation. Figure 1 shows all important parameters that may have an impact on the jet/cavity interaction including the jet parameter, the cavitation parameter and the geometry parameters. Figure2 shows the criterion for the jet/cavity closure interaction mechanism by Paryshev and Money and the improved criterion for the cavity gas-leakage pattern under jet effects. Obviously, the parameter $\bar{J}$ and $\bar{P}$ represent implicitly the jet strength in the above criterions, but other parameters, like nozzle geometry and relative position, are not reflected in the discrimination mechanism. Therefore we try to expand Paryshev's theory and enrich the dimensionless parameters to describe the jet/cavity interaction, in order to build criterions for the different interface evolution mechanism change.
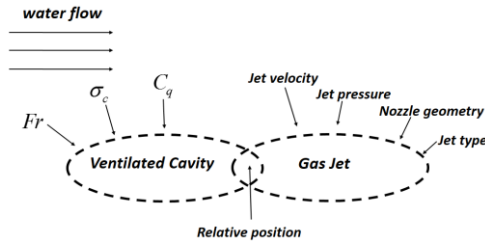

Fig. 1. Key parameters in the jet/cavity interaction.

First of all, the correlation between two non-dimensional numbers $\bar{P}$, $\bar{J}$ and the ratio of the nozzle exit area to the cavitator bottom area is derived.

According to drag and mass flow rate formula equations, we could primitively get:

$$W_c = \frac{1}{2}\rho_\infty U_\infty^2 S_D C_x \tag{6}$$

$$\dot{m}_{jet} = \rho_{jet} U_{jet} S_{jet} \tag{7}$$

In those relations, S_D and S_{jet} denote the cone cavitator bottom area and the nozzle exit area respectively. In combination with Eqs.(4) and (5), furthermore, we could get:

$$\bar{J} \cdot \bar{P} = \frac{2}{C_x}\frac{S_{jet}}{S_D} \tag{8}$$

The above relation shows that the effect of dimensionless nozzle exit area is reflected implicitly by the important parameter $\bar{J}$ and $\bar{P}$. Despite all this, it could provide some meaningful advice for supercavity vehicle design. When thrust ($\bar{J}$) is constant, we should improve S_{jet} / S_D to insure $\bar{P}>1$, so that the cavity is steady based on

Paryshev's theory. Figure 3 shows the improved criterion for the cavity gas-leakage pattern under jet effects. Figures 4 and 5 shows the gas-leakage pattern in different mechanisms, when $\bar{P}>1$, gas leaks out of the cavity in the way of the axial flow pattern; when $\bar{P}<1$, gas leaks out of the cavity in the way of the periodic pulsation pattern.

2.2 Review of Jet Dynamic

In order to understand the internal flow field structure of the cavity with a strong jet, we firstly review of gas jet dynamic knowledge. In general, the jets are classified into two types: free jet and confined jet (as shown in the figure 6 and 7) on the basis of the surrounding environment's effects. The free jet, often exists in an unlimited space and acts as a turbulent free jet. In this paper, we use a circle exit of the converging nozzle. Previous experimental research by Albertson *et al.* (1950) and Schwarz (1963) on the gas jet shows that, when the jet leaves from the orifice and enters into a quiescent environment, the velocity gradient results in the generation of turbulence eddies, and the jet would entrains the surrounding gas and moves forward together. Meanwhile, jet boundary spreads freely in the radial direction. The whole jet development process is composed of two parts: the zone of flow establishment and the zone of established flow. Near the nozzle exit, a triangular area which is not affected by the entrainment and still maintain the original exit velocity is defined as the potential core. The regions between the potential core and the jet boundary is often called the shear layer (or mixing layer). The potential core length (L_1) depends on the geometry shape of convergent nozzle exit.

$$L_1 = 0.671\frac{D_{jet}}{2a} \tag{9}$$

Where D_{jet} is the diameter of the nozzle exit, and a is the turbulence coefficient which could be obtained through experiment, it is often given as a range value of 0.053~0.071 for circle nozzle.

For a confined jet, Kandakure *et al.* (2008) and Ball *et al.* (2012) studied on the jet behavior. A recirculation flow pattern is established because the amount of surrounding gas is not enough for the entrainment in presence of tank wall. Therefore, the jet radius firstly increases and then decreases. The jet boundary is featured and has experienced three stages: free expansion (section I to section II), restricted expansion (section II to section III), and contraction (section III to section IV). The presence of the walls will lead to the higher shear rates which increases the turbulence than that of free jet. Behind the recirculation region, the flow filed turns into the turbulent vortex region. The whole recirculation region length (section I to section IV) L_2 is:

$$L_2 = 3.58\sqrt{A} + \frac{D_{jet}}{a}(0.147\frac{\sqrt{A}}{D_{jet}} - 0.133) \tag{10}$$
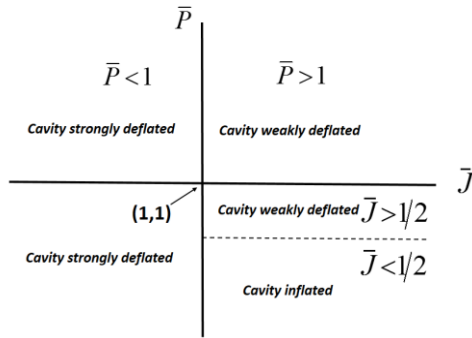
Fig. 2. Criterion for the jet/cavity closure interaction mechanism by Paryshev and Money.
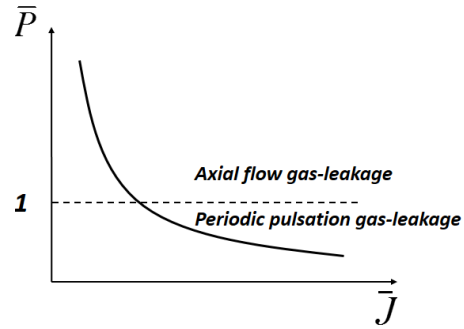

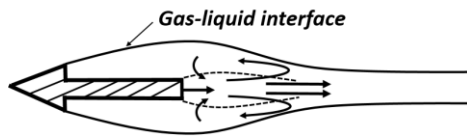**Fig.3. Improved criterion for the cavity gas-leakage pattern under jet effects.**

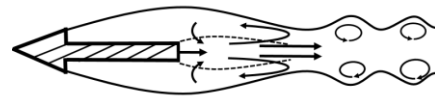**Fig. 4. Structure of the cavity closure onto a central jet of $\bar{P}>1$**

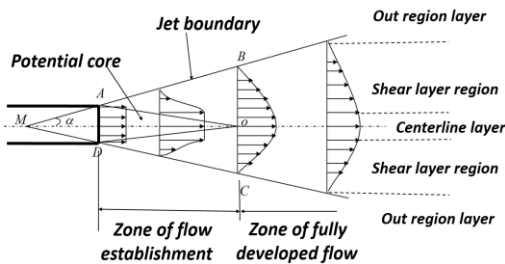**Fig. 5. Structure of the cavity closure onto a central jet of $\bar{P}<1$.**

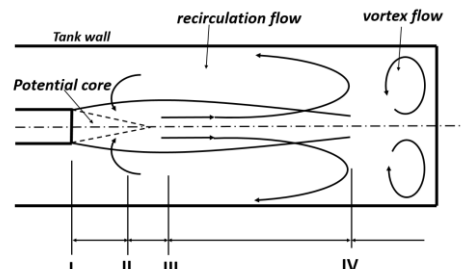**Fig. 6. Schematic of the turbulent round free jet.**

Fig. 7. Schematic of the turbulent round confined jet.

Where A denotes the cross sectional area of the external tank wall.

The above jet dynamic knowledge could help us to understand jet/surpercavity interaction. The jet structure inside the cavity is similar to the confined jet, the only difference is that cavity interface is not fixed walls and relates to complex interface evolution. In one word, gas leakage ways induced by jet entrainment and cavity interface instabilities jointly determine the interface evolution mechanism. Under certain circumstances the jet entrainment would result in the atrophy of the cavity when the cavity doesn't have enough gas to maintain the cavity shape. On the one hand, the intensity of the entrainment effect is related to the jet strength. For an established supercavity, when jet momentum $\bar{J}$ is small, and the velocity gradient is low, the jet couldn't bring gas away from the cavity. As $\bar{J}$ increases to a certain value, due to the enhancement in velocity gradient shear, the jet starts to entrain surrounding gas and leave from the

cavity together. The more gas that maintains the cavity are brought away, the more the cavity shrinks. As $\bar{J}$ continues to increase, the strengthened entrainment effect may result in a pinch-off, pulsating, and unsteady supercavity.

On the other hand, the strength of the entrainment effect is also related to the relative position. When the nozzle exit is nearer to the cavity closure, the shear layer (or mixing layer) zone of jet would diminish. It means that the surrounding gas entrained by jet decrease and may mitigate the negative effects caused by the jet.

2.3 Several Situations of Jet/Cavity Interaction

For an established supercavity and a constant-$\bar{J}$ jet, the distance between the jet nozzle exit and the point of cavity closure (S_0) is speculated to be an important parameter that impacts surface evolution mechanism for the cavity. However, in view of the
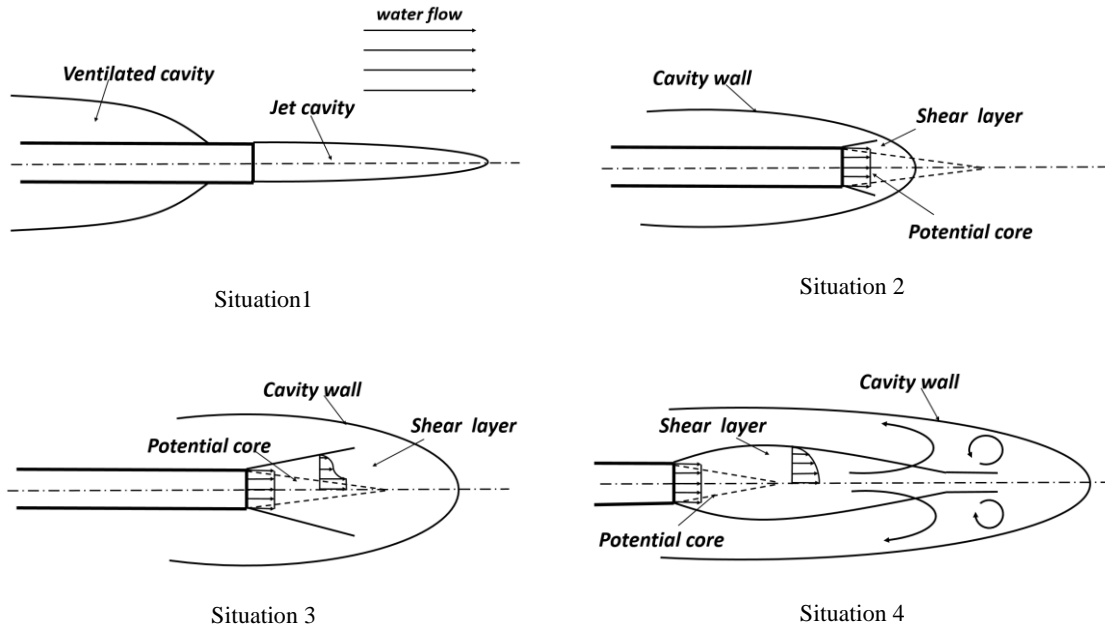
Situation1

Situation 2

Situation 3

Situation 4

Fig.8. Criterion for the jet/cavity interaction mechanism of varying relative position.

asymmetric characteristics of the cavity surface at low *Fr* number, the jet would firstly interact with the lower cavity surface, rather than the closure region due to the buoyance effect, so we redefine the distance parameter which represents the relative position of jet/cavity, that is the axis length of the nozzle outlet to the lower cavity surface. We also give the normalized form as:

$$\overline{S_0} = S_0 / D_n \tag{11}$$

When the relative position varies, several situations of jet/cavity interaction are analyzed as follows, Situation 1: the ventilated cavity closes on the slender body and has little connection with the tail cavity induced by jet.

Situation 2: when $0 < S_0 < L_1$ (or $0 < \overline{S_0} < L_1/D_n$), the nozzle exit is nearer to the cavity closure and the cavity tail closes in the jet's potential core, the jet entrainment effect in cavity is very weak and almost negligible.

Situation 3: when $L_1 < S_0 < L_2$ (or $L_1/D_n < \overline{S_0} < L_2/D_n$), the cavity tail closes at the location outside the potential core, the jet entrainment effect is enhanced.

Situation 4: when $S_0 > L_2$ (or $\overline{S_0} > L_2/D_n$), the entire shear area of the jet is covered by the cavity, and the jet would entrain intensively the surrounding gas from the cavity. We focus on Situation 2 to Situation 4 in our research. The strong entrainment and dissipation of turbulent vortexes bring about the internal pressure and velocity pulsation inside the cavity, eventually resulting that the cavity fail to maintain a stable state, thus requiring the formation of a new interface state.

3. NUMERICAL METHODS

3.1 Computational Methodology

In this manuscript, we use a homogeneous multiphase model based on FLUENT platform. A single set of momentum equations is shared by the fluids, and all material properties of the fields would be determined by the component phases, so long as the volume fraction of each phase is calculated at each control cell. There are two phases in the fluid field, an incompressible liquid phase for the external field and an incompressible non-condensable gas phase for the ventilation and jet. The liquid-gas interface is captured by a method which coupled VOF with level set. It is reasonable cognition that surface tension and turbulence model is important, the classical standard k-epsilon model and surface tension model are used in our simulation.

3.1.1 Governing Equation

The governing continuity equation and momentum equation of a homogeneous multiphase flow are given as follows:

$$\frac{\partial \rho}{\partial t} + \frac{\partial}{\partial x_i}\left(\rho u_i\right) = 0 \tag{12}$$

$$\frac{\partial(\rho_m \boldsymbol{u})}{\partial t} + \nabla \bullet (\rho_m \boldsymbol{u}\boldsymbol{u}) = -\nabla p + \nabla \bullet [\mu_m(\nabla \boldsymbol{u} + \nabla \boldsymbol{u}^{\mathrm{T}})] + \rho_m \boldsymbol{g} + \boldsymbol{F}_s \tag{13}$$

The density and viscosity coefficient of the mixture phase respectively is:

$$\rho_m = \rho_l(1-\alpha_g) + \rho_g \alpha_g \tag{14}$$

$$\mu_m = \mu_l(1-\alpha_g) + \mu_g \alpha_g \tag{15}$$

1327

Where α_g represents the volume fraction of gas phase, on the other hand $1-\alpha_g$ could represents the volume fraction of liquid phase.

3.1.2 Coupled VOF and Level Set Method:

In the method of coupled VOF and level-set (CLSVOF) proposed by the Bourlioux (1995) and Sussman and Puckett (2000), the interface is captured and tracked by solving the volume fraction equation and level-set function together. The main idea is to benefit from the advantage of each strategy, which is to ensure mass conservation with the VOF method and to keep a fine description of the geometrical properties of the interface by the level set method. And the volume fraction equation for the gas phase is given as follows:

$$\frac{\partial \alpha_g}{\partial t} + \nabla \bullet (\boldsymbol{u}\alpha_g) = 0 \tag{16}$$

The cell domain of $0 < \alpha_g < 1$ contains the interface between the gas phase and the liquid phase.

The level-set function $\varphi(x,t)$ is defined as a signed distance between any point in the field and the interface. Accordingly, the interface is the zero level-set, $\varphi(x,t)$ and can be expressed as $\Gamma = \{x \mid \varphi(x,t) = 0\}$ in a two-phase flow system:

$$\varphi(x,t) = \begin{cases} +|d|, & x \in \text{the primary phase} \\ 0 & , & x \in \Gamma \\ -|d|, & x \in \text{the second phase} \end{cases} \tag{17}$$

Where d is the distance from the interface. In a given velocity field $\boldsymbol{u}$, solving a convection equation determines the evolution of the interface:

$$\frac{\partial \varphi}{\partial x} + \nabla \bullet (\mathbf{u}\varphi) = 0 \tag{18}$$

By nature of the transport equation of the level-set function Eq. (18), it is unlikely that the distance constraint $|\nabla \varphi| = 1$ of is maintained after its solution. A re-initialization process is therefore needed for each time step. The geometrical interface construction method which is reliable on the values of the VOF and the level-set function is used here to reconstruct the interface. Namely, the VOF method provides the size of the cut in the cell where the likely interface passes through, and the gradient of the level-set function determines the direction of the interface.

3.1.3 Surface Tension Model

In momentum Eq.(13), $\boldsymbol{F}_s$ is the force arising from surface tension effects given by:

$$\boldsymbol{F}_s = \sigma\kappa\delta(\varphi)\boldsymbol{n} \tag{19}$$

Where σ is the surface tension coefficient and

equals to 0.072N/m at normal temperature. And $\delta(\varphi)$ function is defined as:

$$\delta(\varphi) = \begin{cases} 0, & |\varphi| \ge \varepsilon \\ \dfrac{1+cos(\pi\varphi/\varepsilon)}{2\varepsilon}, & |\varphi| < \varepsilon \end{cases} \tag{20}$$

Where ε is the thickness of the gas-liquid interface. The normal, $\boldsymbol{n}$, and curvature, κ, of the interface can be given as:

$$\kappa = \nabla \cdot \frac{\nabla \varphi}{|\nabla \varphi|}\bigg|_{\varphi=0}, \qquad \boldsymbol{n} = \frac{\nabla \varphi}{|\nabla \varphi|}\bigg|_{\varphi=0} \tag{21}$$

3.2 Physical Model, Mesh and Boundary Condition Description

The object of simulation which used to research on jet/cavity interaction is derived from Money's experimental model (2015). The model consists of a 30-degree, 31.75mm diameter cone cavitator at the head of the slender body and a converging circular nozzle in the rear. The model has the geometrical characteristic of large cavitator, short body and small nozzle exit, the ratio of nozzle exit area to cavitator bottom area, S_{jet} / S_D, is approximately equal to 0.12. We know that it is easy to form unsteady supercavity flows with a strong gas jet from the previous analysis. In order to investigate the effect of relative position, we have designed four different length size for the simulation model.

The computational mesh is showed in Fig.10. Grid refinement is carried out around the physical model body and in the nozzle tail domain. The number of mesh nodes is 1.7 million after mesh adaption analysis, which can better capture the interface variation of the cavity and the development of the jet morphology.

The boundary conditions are applied as follows: the velocity inlet and pressure outlet boundary conditions are used for the distribution of the incoming flow and outlet boundary, and the symmetric boundary condition is used for the symmetric surface. The non-slip wall boundary condition is used for the physical mode wall and the slip wall boundary condition is use for the far field. The ventilation and jet ports use mass flow inlet boundary.
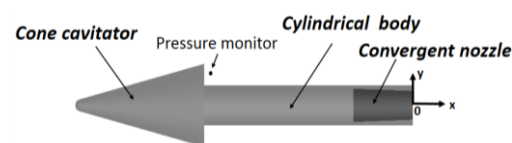

Fig. 9. Physical model of simulation.

3.3 Validation for a Supercavitating Case

Firstly we have done a validation work of steady supercavity without jet by comparing the CFD results with theory data. Guzevsky (1973) gave empirical formulas for the supercavity length,
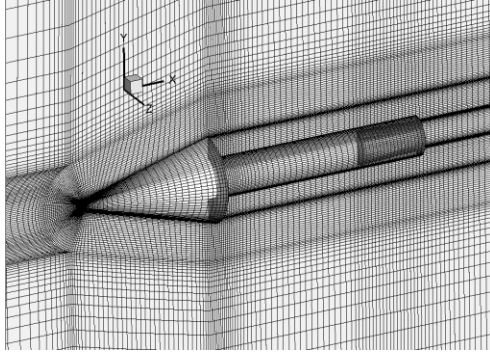
maximum diameter and drag coefficient of cone cavitator.

Fig. 10. The computational mesh.

$$D_c = D_n \sqrt{\frac{C_x}{k\sigma_c}} \tag{22}$$

$$L_c = D_n \left[\frac{1.1}{\sigma_c} - \frac{4(1-2\alpha)}{1+144\alpha^2} \right] \sqrt{C_x \ln \frac{1}{\sigma_c}} \tag{23}$$

$$k = \frac{1+50\sigma_c}{1+56.2\sigma_c} \tag{24}$$

$$C_x = C_{x0} + (0.524 + 0.672\alpha)\sigma_c \quad 1/12 \le \alpha \le 1/2 \tag{25}$$

$$C_{x0} = 0.5 + 1.81(\alpha - 0.25) - 2(\alpha - 0.25)^2 \quad 1/12 \le \alpha \le 1/2 \tag{26}$$

Where *Dc* and *Dn* are the theoretical maximum diameter of the supercavity cross section and the diameter of the cone cavitator; *Cx* represents the drag coefficient of the cone cavitator, *Cx0* is the drag coefficient when cavitation number equals zero. $\pi\alpha$ is the half top angle of a cone, so $\alpha = 1/12$ in this paper.

As shown in Fig.11 and table 1, under different ventilation flow rate, the average relative errors of the comparisons in the cavity maximum diameter, length and the drag coefficient are 2.25%, 8.7% and 5.1%, respectively.

4. NUMERICAL RESULTS AND DISCUSSIONS

In order to study the effect of $\bar{S}_0$ on jet/supercavity interaction, one way is to change the ventilation rate or the free stream velocity so that the cavity closure region closes to the nozzle exit, the other way is to elongate the model's body to make that the nozzle exit closes to the cavity closure region. We choose the latter because that could avoid introducing other variables when different $\bar{S}_0$ is analyzed. We firstly simulate a steady cavity in the condition of *Fr*=11.4, *Cq*=0.16. And then a strong jet with strength of $\bar{J}$ =1, $\bar{P}$ =1.355 and $\bar{J}$ =1.88, $\bar{P}$ =0.72 is generated. Thereafter, by changing the relative position of nozzle exit to the cavity with four different length of physical models, a series of numerical simulation of supercavitating flows is

performed as shown in.

According to formula Eq. (9), the dimensionless jet potential core length is obtained：

$$L_1/D_n = \frac{0.671}{2a} \frac{D_{jet}}{D_n} \tag{27}$$

According to formula Eqs. (10) and (22), where *A*, the cross sectional area in the confined space is decided by the maximum cross sectional area of the cavity, the dimensionless recirculation region length of the jet is obtained：

$$L_2/D_n = (3.58 + \frac{0.147}{a})\sqrt{\frac{\pi}{8}} \frac{D_C}{D_n} - \frac{0.133}{a} \frac{D_{jet}}{D_n} \tag{28}$$

The theoretical value of L_1/D_n and L_2/D_n are 2.19 and 6.4 respectively. Figure 12 shows four groups of the relative position between nozzle exit and cavity. Combined with the discriminant criterion for the jet/cavity interaction mechanism with varying relative position (Fig. 8), these calculation cases could be reasonably classified: the case 1a, case 1b, case 2a and case 2b belong to situation 4, the case 3a and case3b belong to situation3, and the case 4a and case4b belong to situation 2.

4.1 The cavity Interface Evolution Process

Figures 13 and 14 show respectively the cavity interface transient evolution process for case 1b

($\bar{P} < 1$ and $\bar{S}_0 > L_2/D_n$) and case 4b ($\bar{P} < 1$ and $\bar{S}_0 < L_2/D_n$). For case1b, a comparison is shown between CFD predictions and Money's experiment results (2015). The numerical methods are proved to be accurate in capturing interface motion for the cavity. It can be clearly seen from the CFD results that the cavity bubble pinch off and shed due to elongated morphology, while in the experiment, because of the strong instability of gas-liquid interface and the mixing of water and gas, a large number of continuous broken bubbles are actually observed.

The cavity interface evolution process could be subdivided into two stages according to present simulation and experiment dates. During the first stage, the cavity experiences an expansion, necking, and shedding process with jet effects. The total cavity gets a reduction in volume by retraction, which is showed as the elastic behavior of cavity interface. Then, for the second stage, the cavity presents periodic gas-leakage in the tail and maintain this unsteady state of affairs continued. But for case 4b, the first stage is not obvious, after a period of temporary the cavity begins directly to leak gas in the way of the periodic pulsation pattern. The difference between two situations is that the former exists a fluid thread breakup phenomenon drove by the Plateau-Rayleigh instability explained by Eggers (1997), which is characterized by the elongation of the fluid shape forming thin, thread-like regions between larger nodules of fluid.
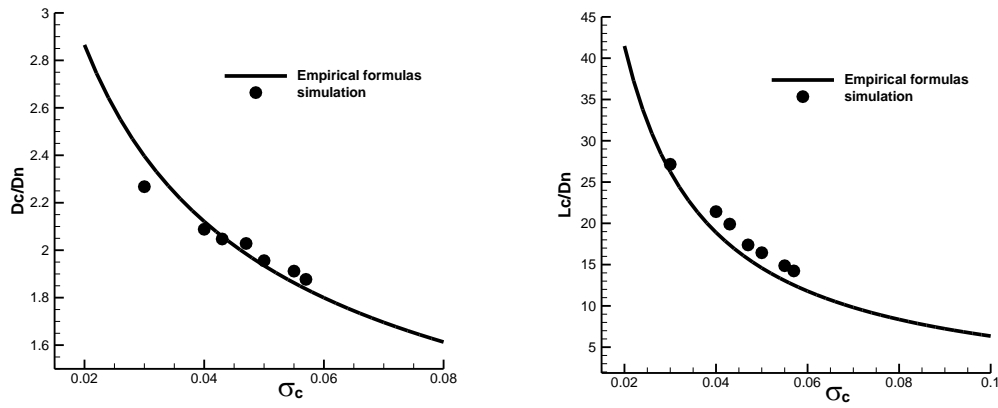
Fig. 1. Dimensionless maximum diameter and length of the cavity at different cavitation number.

Table 1 Drag coefficient of 30-degree cone cavitator

Ventilation coefficient	Cavitation number	CFD results Cx	Theory results Cx
0.12	0.057	0.177	0.176
0.16	0.055	0.177	0.175
0.32	0.050	0.175	0.172
0.64	0.047	0.178	0.170
0.96	0.043	0.179	0.168
1.28	0.040	0.180	0.167
2.56	0.030	0.188	0.160

Table 2 Calculation cases of jet/cavity interaction with different relative position

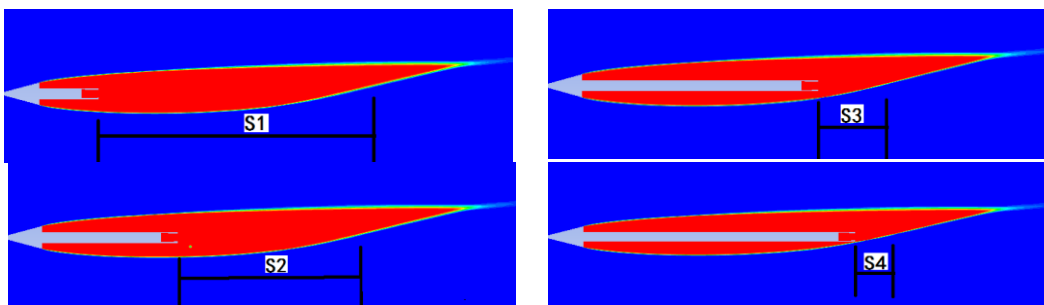| *case*	U_∞ *(m/s)*	Q_D *(kg/s)*	$\dot{m}_{jet}$ *(kg/s)*	$\overline{J}$	$\overline{S}_0$
Case 1a	6.36	0.00062328	0.00908307	1	10.90
Case 1b	6.36	0.00062328	0.0124656	1.88	10.90
Case 2a	6.36	0.00062328	0.00908307	1	7.56
Case 2b	6.36	0.00062328	0.0124656	1.88	7.56
Case 3a	6.36	0.00062328	0.00908307	1	2.83
Case 3b	6.36	0.00062328	0.0124656	1.88	2.83
Case 4a	6.36	0.00062328	0.00908307	1	1.26
Case 4b	6.36	0.00062328	0.0124656	1.88	1.26

Fig. 2. Relative position between nozzle exit and cavity.

breakup of the fluid into small packets to minimize the system surface energy by reducing the surface area. Especially, the changes of the cavity length needs to be concerned. Further research is needed to make certain when the cavity would experience pinch-off. The distance parameter $\overline{S}_0 = L_2/D_n$

may be the critical point.

In the cavity interface evolution process, two special moments are emphatically analyzed. The moment of t=0.15s is that the cavity forms the final shape in the periodic varying state of growth and shedding. And the moment of t=0.005s is that the
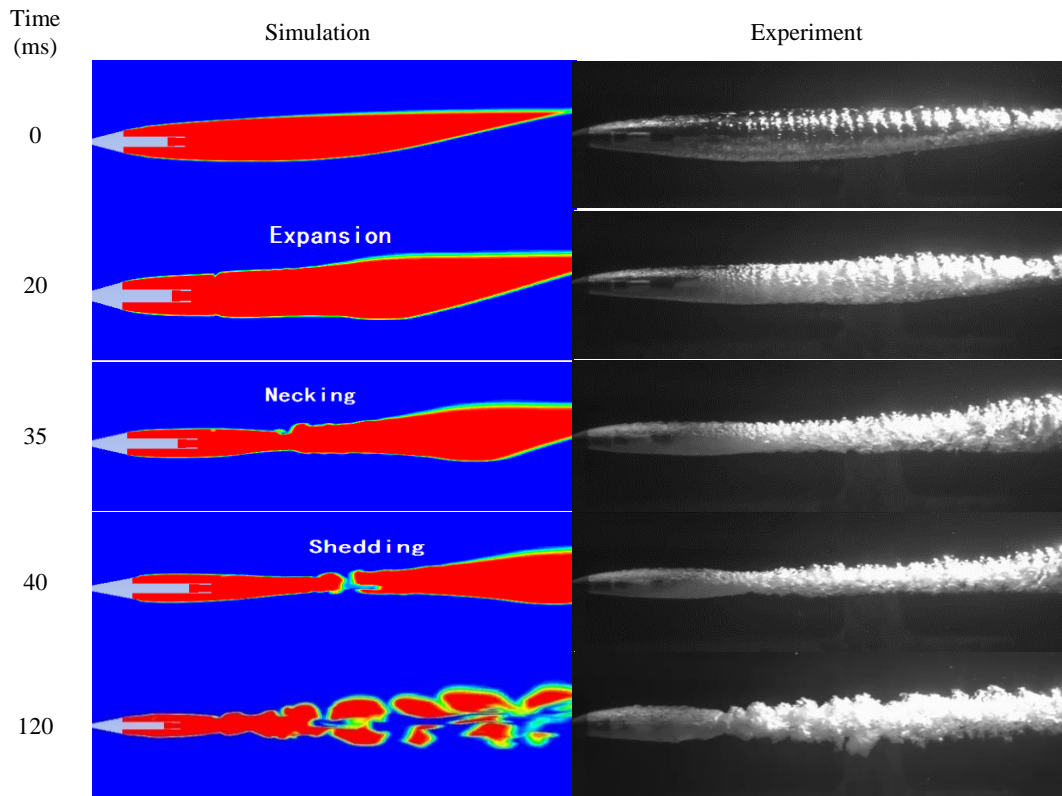
Fig. 3. Cavity interface evolution showed by the contours of volume fraction when $\bar{P}<1$ **and** $\overline{S_0} > L_2/D_n$ **(blue regions: water, red regions: gas).**
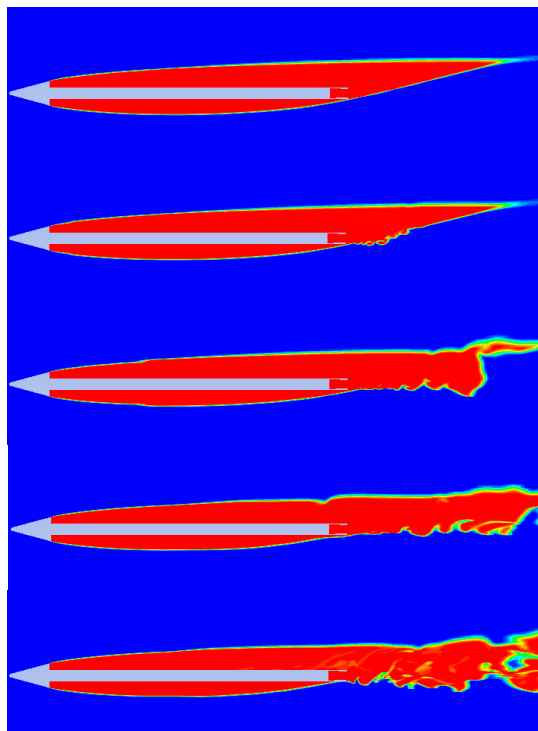

Fig. 4. Cavity interface evolution when $\bar{P}<1$ **and** $\overline{S_0} < L_2/D_n$**.**

jet has just formed but the cavity shape has not changed yet. Clearly describing the structural characteristics of the confined jet, the strength of the entrainment effect and it's influence on the quality change inside the cavity at this moment, that is meaningful to study the evolution mechanism of the cavity interface.
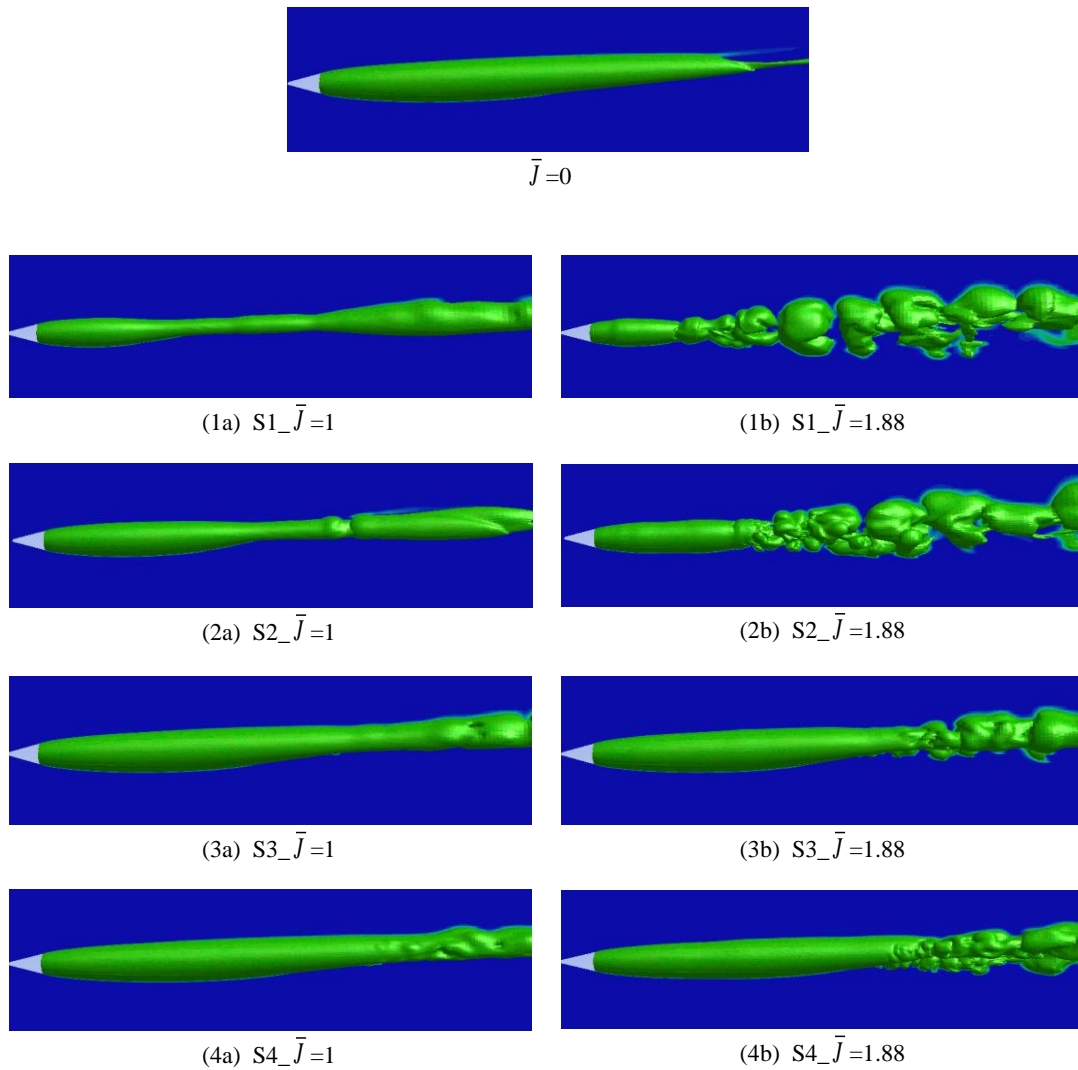
$\bar{J}=0$

(1a) S1_$\bar{J}=1$

(1b) S1_$\bar{J}=1.88$

(2a) S2_$\bar{J}=1$

(2b) S2_$\bar{J}=1.88$

(3a) S3_$\bar{J}=1$

(3b) S3_$\bar{J}=1.88$

(4a) S4_$\bar{J}=1$

(4b) S4_$\bar{J}=1.88$

Fig. 5. Cavity morphology characteristics for varying relative position and jet strength at T=0.15s. The cavity interface is obtained by gas volume fraction of 0.5. Left : $\bar{P}>1$ and right : $\bar{P}<1$.

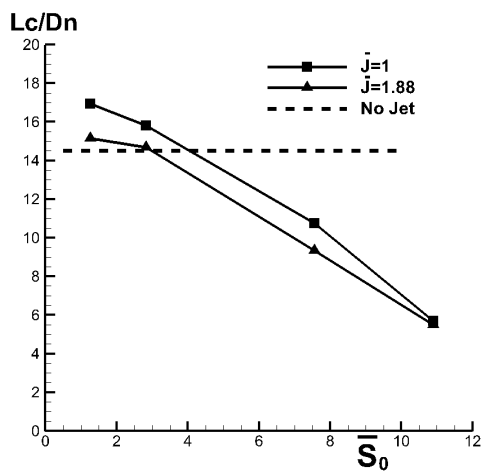**Fig. 6. Dimensionless cavity length as the distance parameter varies.**

Figure 15 shows the cavity morphology characteristics for varying relative position and jet strength at T=0.15s. It is concluded that, when $\bar{P}>1$, the periodic gas-leakage phenomenon is not obvious, the cavity deflates in pattern of axial flow (Efros-type) so that the cavity tail looks slender; when $\bar{P}<1$, distinct periodic pulsation in the tail is observed. As for the influence of the relative position, the pinch-off phenomenon in the cavity interface evolution is observed for case S1 and case S2, but for case S3 and case S4, it turns to be not obvious. Figure 16 shows the dimensionless cavity length as the distance parameter varies. As the distance parameter $\bar{S}_0$ decreases, the cavity length shows a trend of increase. When the nozzle outlet is far from the cavity tail as in case S1 and case S2, an obvious shrinkage is resulted from the jet. However, when the nozzle moves closer to cavity tail, a slightly expansion is generated by the jet. It is
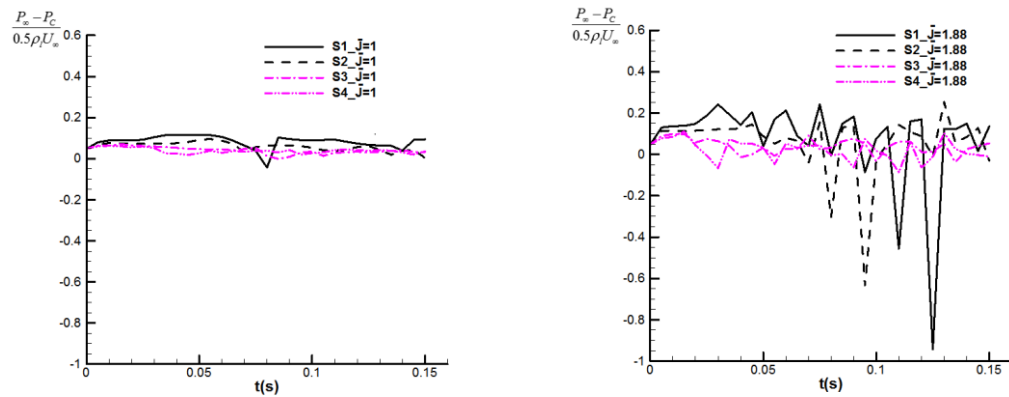
1332

Fig. 7. Pressure pulsation characteristics inside the cavity for different relative position and jet strength.

S1_$\bar{J}$ =1.88

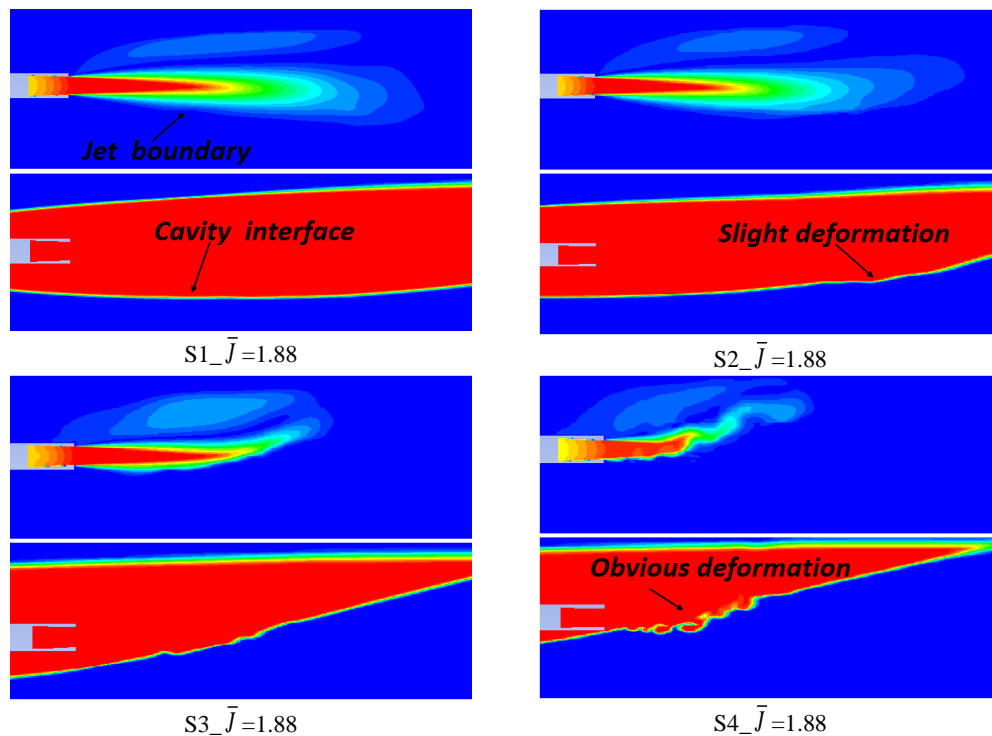S2_$\bar{J}$ =1.88

S3_$\bar{J}$ =1.88

S4_$\bar{J}$ =1.88

Fig. 8. As the relative position varies, jet boundary and cavity interface interaction are showed at T=0.005s.

the main reason for the variation of the cavity length whether the pinch-off occurs in the cavity interface evolution process. And the critical point $\overline{S_0}$ seems like to be smaller than L_2/D_n in the Fig.16. From the view of the cavity instability with internal jet perturbations, case S1 with $\bar{J}$ =1.88 is the most unstable, which has distinct interface fluctuation, and strong shrinkage. The weakest jet perturbation is in case S4 with $\bar{J}$ =1, which has the most stable state. Figure 17 shows pressure pulsation characteristics inside the cavity for different relative position and jet strength (Pressure monitoring points are selected near the cavitator showed in Fig.9). In the process of unsteady gas-leakage, the cavity would present periodic expansion and shedding. When the cavity varies in

the process of expansion, the pressure would decrease. At the moment of shedding, the pressure changes quickly that behaves as a broken line for the pressure cure. When $\bar{P}>1$, the pressure fluctuation is small because the cavity is relatively stable in the axial flow gas-leakage pattern; when $\bar{P}<1$, the pressure fluctuation is really strong due to the unstable periodic pulsation pattern.

4.2　The confined Jet Structure in a Variable Cavity

The jet spreads inside the cavity, which will result the fluctuation and deformation of the cavity surface. On the other side, the change of the cavity will also give rise to variation of the jet style due to the change of the ambient flow parameters. Figure 18 shows the interaction between jet boundary and
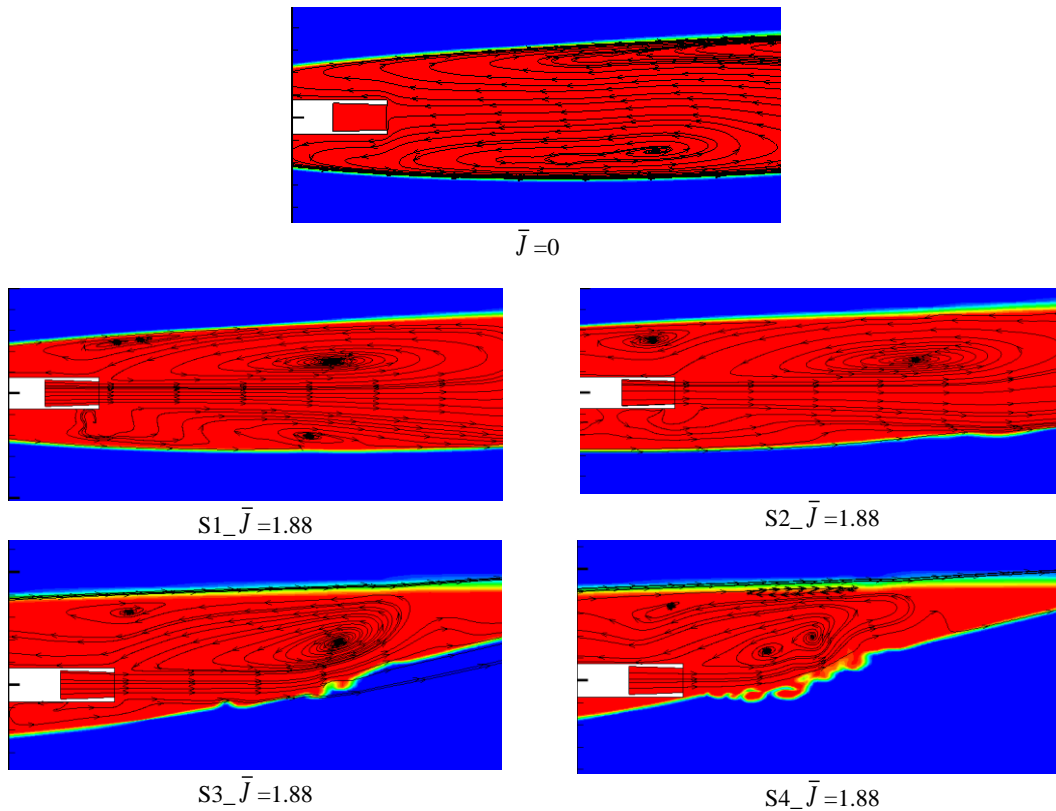
$\overline{J}=0$

S1_$\overline{J}=1.88$

S2_$\overline{J}=1.88$

S3_$\overline{J}=1.88$

S4_$\overline{J}=1.88$

Fig. 9. As the relative position varies , the velocity streamline inside the cavity is showed at T=0.005s.

cavity interface as the relative position varies at T=0.005s. As the distance parameter $\overline{S_0}$ decreases, jet structure turns from a symmetrical and fully developed jet into an asymmetrical and developing jet. The cavity interface evolves from no fluctuations, slight deformation, enhanced deformation to obvious deformation.

Figure 19 shows velocity streamline diagram in the cavity flow field with a gas jet as the distance parameter varies. Before the jet is generated, the gas near the gas-liquid interface is dragged by the water flow, the internal cavity appears backflow. After the jet is triggered, the internal cavity flow is dominated by the jet and the vortex direction is changed. In case S1, due to asymmetrical entrainment effect by the jet, the cavity has asymmetrical vortex structure, and the gas dragged by the external water flow and re-entrant jet conspire to form a small vortex in front. In case S2, the vortex in the lower side of the cavity almost disappears. In case S3 and case S4, the vortex structure is obviously limited by the narrow space. In particular, instead of a big vortex, it becomes vortex pair is in case S4。

Figure 20 shows the normalized centerline axial velocity decay of the jet for varying relative position and jet strength at T=0.005s. As for case S1 and case S2, the jet structure is a symmetrical and fully developed type, which is weakly disturbed from the downside cavity wall. By considering momentum balance, the entrainment effect of case S1 is stronger than that of case S2, so that the centreline axial mean velocity decay faster in case

S1. But for case S3 and case S4, the jet structure is an asymmetrical and developing type, which encounters with the stagnation effect from external water fluid, so the centreline axial mean velocity decay dramatically.

Table3 shows the basic parameters of the confined jet structure, dimensionless potential core length and recirculation region length for varying relative position. In case S1, case S2 and case S3, the potential core length of the jet are almost equal to the theoretical value, but for case S4, the potential core length is smaller than the theoretical value for $0 < \overline{S_0} < L_1/D_n$. In case S1 and case S2, the recirculation region length of the jet are approximate to the theoretical value, but for case S3 and case S4, the potential core length is smaller than the theoretical value for $\overline{S_0} < L_2/D_n$.

4.3 Quantitative Analysis of the Entrainment Effect

Figure 21 shows the theoretical cavity internal structure with a gas jet. Qx denotes the mass flow rate across the jet section. $\dot{m}_{jet}$ and Q_D denotes the mass flow rate of the jet nozzle and ventilation respectively. Jet entrainment effect results in a recirculation flow in the cavity interior and builds a new gas-leakage pattern in the cavity tail. Q_R is the reflux mass flow rate. The entrainment mass flow rate could been obtained by subtracting the mass flow at the nozzle exit from the mass flow at the jet cross section ($Q_x - \dot{m}_{jet}$).
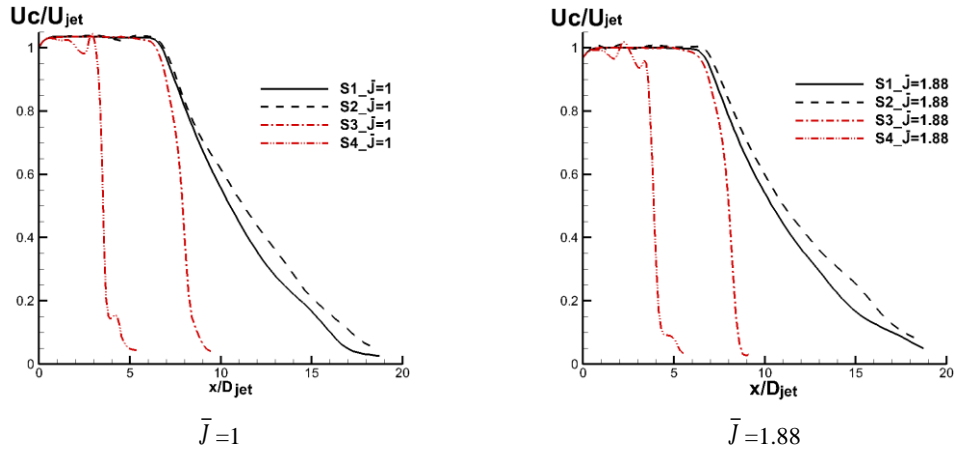
$$\bar{J}=1 \qquad\qquad \bar{J}=1.88$$

Fig. 10. Normalized centerline axial mean velocity decay at T=0.005s.

Table 3 Dimensionless potential core length and recirculation region length of the jet at T=0.005s

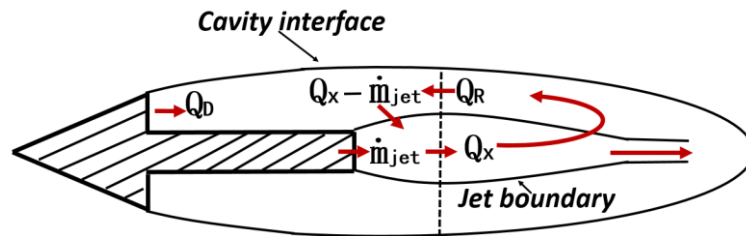| Jet parameter	L_1/D_n	L_2/D_n
Theory results	2.19	6.4
Case 1a	2.24	5.86
Case 1b	2.20	6.20
Case 2a	2.33	6.30
Case 2b	2.30	6.23
Case 3a	2.30	4.19
Case 3b	2.20	4.31
Case 4a	1.32	3.15
Case 4b	1.29	3.40

Fig. 21. Schematic of the cavity internal flow structure with a gas jet.

Figure 22 shows the normalized entrainment rates of the surrounding gas into the jet for varying relative position and jet strength at T=0.005s. Along the axial direction, the entrainment rate firstly increases to a peak value and then decreases. For all cases, the maximum entrainment rate appears at the maximum radius of the jet. It can be seen that the stronger the jet is, the larger the entrainment rates are. The entrainment rates also reduce with the decrease of the relative position $\overline{S_0}$. The non-dimensional parameter $\bar{J}$ and $\overline{S_0}$ jointly determine the entrainment intensity.

Table 4 shows the entrainment and recirculation mass flow rate at the max jet radius for each case at T=0.005s. Therefore we could make a quantitative

analysis to indicate the morphological changes of the cavity. Analyzing the change of gas mass in the forepart of the cavity by calculating the max entrainment flow rate plus ventilation and recirculation flow rate, we could judge whether the cavity will be depressed or expanded at the next time step. When $Q_x - \dot{m}_{jet} - Q_D - Q_R > 0$, it deflates the cavity so that the cavity will get smaller; when $Q_x - \dot{m}_{jet} - Q_D - Q_R < 0$, it inflates the cavity so that the cavity volume will become larger.

The cavity interface evolution process are also the rebuilding process from an unbalance state to a dynamic balance state, in which the beginning state is $Q_x - \dot{m}_{jet} - Q_D - Q_R > 0$ or < 0, and the ending
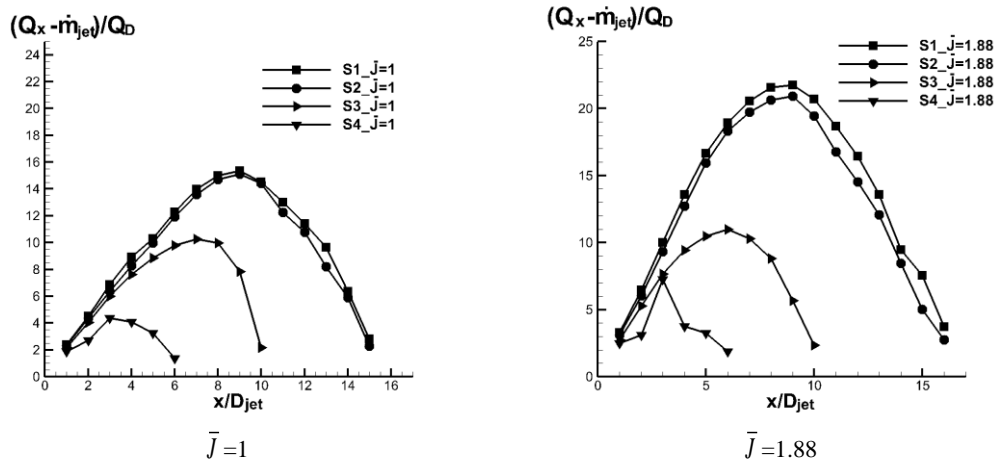
$\bar{J} = 1$ $\bar{J} = 1.88$

Fig. 11. Normalized entrainment rates of the surrounding gas into the jet along the axial direction at T=0.005s.

Table 4 The entrainment and recirculation mass flow rate for each case at T=0.005s. The max entrainment mass flow rate is obtained at the max jet radius. The dates in the table are half of the actual value for one half of computational domain

Case	Ventilation flow rate Q_D (kg/s)	Jet flow rate $\dot{m}_{jet}$ (kg/s)	The maximum entrainment flow rate $Q_x - \dot{m}_{jet}$ (kg/s)	Recirculation flow rate Q_R (kg/s)	$Q_x - \dot{m}_{jet} - Q_D - Q_R$
S1_$\bar{J}$=1	0.00062328	0.00908307	0.00956197	0.0088959	>0
S2_$\bar{J}$=1	0.00062328	0.00908307	0.00941998	0.0086789	>0
S3_$\bar{J}$=1	0.00062328	0.00908307	0.00638417	0.0079659	<0
S4_$\bar{J}$=1	0.00062328	0.00908307	0.00273304	0.0045968	<0
S1_$\bar{J}$=1.88	0.00062328	0.0124656	0.0135627	0.0123124	>0
S2_$\bar{J}$=1.88	0.00062328	0.0124656	0.0133854	0.0114708	>0
S3_$\bar{J}$=1.88	0.00062328	0.0124656	0.0068512	0.0084827	<0
S4_$\bar{J}$=1.88	0.00062328	0.0124656	0.0045186	0.0067525	<0

state is the mass flow balance inside the cavity that $Q_x - \dot{m}_{jet} - Q_D - Q_R \approx 0$ for $\bar{P} > 1$, or the arithmetic mean value in one period approximately equal to zero for $\bar{P} < 1$.

5. CONCLUSION

In order to promote the engineering application of supercavitating technology, the jet/cavity interaction was investigated based on numerical methods in this paper. A multiphase model using coupled VOF and level set method is adopted to capture gas-liquid interface. The cavity interface evolution process have been studied and summarized based on simulation and experimental dates.
A series of numerical simulations of supercavitation flows was performed to reveal the jet/cavity interaction mechanism. The transition criterion with varying jet strength and relative position is

proposed and validated. Based on the numerical and theoretical analysis, it is concluded that the non-dimensional parameter $\bar{J}$ and $\bar{S_0}$ jointly determine the entrainment effect intensity. Gas leakage ways induced by jet entrainment and cavity interface instabilities jointly determine the interface evolution mechanism. When $\bar{P} > 1$, gas leaks out of the cavity in the way of the axial flow pattern; and when $\bar{P} < 1$, gas leaks out of the cavity in the way of the periodic pulsation pattern. For $\bar{S_0} > L_2/D_n$, the cavity interface evolution experiences an expansion, necking, and shedding process; and for $\bar{S_0} < L_2/D_n$ the cavity wouldn't experience pinch-off.

Based on the above analysis, the supercavitation vehicles is recommended to improve the ratio of the nozzle exit area to the cavitator bottom area (increase S_{jet}/S_D), make sure that the nozzle outlet is close to the cavity tail (decrease $\bar{S_0}$) and it's

suitable for straight operation under the condition of high speed (increase $\bar{P}$), which tends to build a stable supercavitaion with a strong gas jet from exhaust nozzle.

Finally, a quantitative analysis method has been studied, which is to associate entrainment effect and the cavity interface evolution. In future work, we will try to construct semi-empirical formulas between cavity dimensions and $\bar{J}$, $\bar{S_0}$, Fr , Cq etc, and use a regular active inflation technology to control the mass flow balance inside the cavity for the most unstable cavitation under certain circumstances ($\bar{P} < 1$ and $\bar{S_0} > L_2/D_n$). It should be an important and practical theory in the artificial supercavition technique.

ACKNOWLEDGMENTS

REFERENCES

Albertson, M. L., Y. B. Dai, R. A. Jensen and H. Rouse (1950). Diffusion of submerged jets. *Transactions ASCE*. 115,639-664.

Ball, C. G., H. Fellouah and A. Pollard (2012). The flow field in turbulent round free jets. *Progress in Aerospace Sciences*. 501-26.

Bourlioux, A. (1995). A coupled level-set volume-of-fluid method for tracking material interfaces. In: *Proceedings 6th Annual Int. Symp.on Comp. Fluid Dynamics*, Lake Tahoe, USA.

Eggers, J. (1997). Nonlinear dynamics and breakup of free-surface flows. *Reviews of Modern Physics* 69(3),865-930.

Guzesky, L. G. (1973). Approximation dependences for axisymmetric cavities behind cones. In: Hydrodynamic Flows and Wave Processes (collected scientific papers), Inst. Thermophys, Sib. Branch, Acad. of Sci. of the USSR, Novosibirsk, 92-91.

Henderson, D., W. Pritchard and L. Smolka (1997). On the pinch-off of a pendant drop of viscous fluid. *Physics of Fluids* 9 (11),3188.

Kandakure, M. T., V. C. Patkar and A. W. Patwardhan (2008). Characteristics of turbulent confined jets. *Chemical Engineering and Processing*. 47,1234–1245.

Karn. A., R. E. A. Arndt and J. R. Hong (2016) An experimental investigation into supercavity closure mechanisms. *Journal of Fluid Mech*anics 789, 259-284.

Kinzel, M. P., M. H. Krane, I. N. Kirschner and M. J. Moeny (2017). A numerical assessment of the interaction of a supercavitating flow with a gas jet. *Ocean Engineering* 136, 304-313.

Money, M. J., M. H. Krane, I. N. Kirschner and M. P. Kinzel (2015). Jet-Supercavity Interaction: Insights from experiments. *In: Proceedings of the 9th International Symposium on Cavitation* (CAV2015).

Paryshev, E. V. (2006). Approximate Mathematical Models in High-Speed Hydrodynamics. *Journal of Engineering Mathematics* 55(1–4), 41–64.

Reichardt, H. (1946). *The laws if cavitation bubbles as axially symmetrical bodies in a flow. Britian*: Ministry of Aircraft Production Reports and Translations.

Schwarz, W H. (1963). The radial free jet. *Chemical Engineering Science* 18,779-786.

Sun, T., X. Zhang, C. Xu, G. Zhang, S. Jiang and Z. Zong (2019) Numerical modeling and simulation of the shedding mechanism and vortex structures at the development stage of ventilated partial cavitating flows. *European Journal of Mechanics B-Fluids* 76, 223- 232.

Sussman, M. and E. G. Puckett (2000). A coupled level set and volume-of-fluid method for computing 3D and axisymmetric incompressible two-phase flows. *Journal of Computer Physics* 162, 301-337.

Xu, H., C. Wang, H. Z. Lu and W. H. Huang (2018). Experimental study on submerged supersonic gaseous jet induced tail cavity. *Acta Physica Sinica*. 67,014703.

Zou, W., K. P. Yu and X. H. Wan (2010). Research on the gas-leakage rate of unsteady ventilated supercavity. *Journal of Hydrodynamics* 22(1),736-741.

Zou, W., K. P. Yu, R. E. A. Arndt, G. Zhang and Z. W. Li (2013). On the shedding of the ventilated supercavity with velocity disturbance. *Ocean Engineering* 57, 223-229.